AE Evaluation of Steel-Concrete Bond Strength Induced with Corrosion Damage

AE EVALUATION OF STEEL-CONCRETE BOND STRENGTH INDUCED WITH CORROSION DAMAGE

Yangqiuye Gao, Veronica Page, Hwa Kian Chai, Mike Forde
The University of Edinburgh
School of Engineering
Edinburgh, EH8 9FG
United Kingdom

Jiangfeng Dong
Sichuan University
College of Architecture and Environment
Chengdu, 610065
China

KEYWORDS: Corrosion, Bond Strength, Acoustic Emission, AFSC, DA

ABSTRACT

Corrosion of steel rebar in concrete structures is a common durability problem that leads towards peeling of concrete cover and loss of bond strength between steel and concrete, thus, impairing the stiffness and the integrity of the whole structure. To evaluate the effects of rebar corrosion on steel-concrete bond strength, an experimental campaign was implemented to monitor the acoustic emission (AE) events during static and cyclic pull-out tests. The failure mode and AE signal features during test were analysed to reveal the concrete fracture characteristic and failure behaviour under the pull-out loading. Two AE-based damage parameters, AFSC and DA are proposed in this study to describe the damage procedure during pull-out test.

INTRODUCTION & BACKGROUND

Corrosion of steel bars is one of the common threats faced that has direct implications on the serviceability of reinforced concrete (RC) structures. In the chloride-induced environment, steel corrosion products gradually accumulate and expand inside the concrete, leading to cracking of the concrete cover, thereby impairing the durability of the structures (Stewart, 1998). In the circumstances of continuous damage occurring in RC structures, it is necessary to evaluate the severity of damage in a timely manner. Accurate evaluation can provide robust and supportive information in strategizing for the extension of the life-span of structures by suitable means of repair and strengthening.

There are many non-destructive testing (NDT) methods for structures assessment, such as ultrasonic, infrared, acoustic emission. The acoustic emission (AE) technology is non-invasive and has been applied to the evaluation and diagnosis of various structural types including bridges, buildings, and dams (Golaski et al., 2002, Ohtsu, 1987, Grosse, 1997). Steel rebar is commonly used in concrete structures for achieving stiffness and ductility. The concrete bears compressive stresses while the steel rebar bears tensile stresses from loading. During the process of rebar corrosion, the formation of corrosion products, i.e., the rust, weakens the bond between concrete and rebar, leading to the loss of capacity of rebar in sustaining tensile stresses.

The bond strength during rebar pull-out is affected by various factors such as concrete cover thickness, water-cement ratio, and corrosion degree (Yalciner et al., 2012). Besides, corrosion results in two major failure modes, the concrete splitting and shear failure (Saether, 2011). Compared to tensile fracture, AE signals from shear fracture have a relatively low average frequency and relative high RA values, while acoustic interface signals of solid interface friction have rather lower energy and frequency than the shear fracture (Wang, 2010). During the pull-out of rebar in concrete, resistance against debonding is given by the steel-concrete shear interlock, adhesion, and frictional resistance between rebar and concrete matrix (Nawy, 2000). Once the rebar begin to slip, the adhesion fails, so the friction and shear interlock provide the resistance mainly

From a microscopic point of view, the shear interlock acts as extrusion and shear between the ribs and the concrete. Under the influence of confining pressure or restraint force, two forms of failure will occur, splitting (Park, 1985) or shearing (Saether, 2011).

For splitting cracks, the ribs and the concrete extrude each other under external load. This local extrusion force produces a radial force component p perpendicular to the rebar and a longitudinal component force τ parallel to the rib surface inside the concrete, as shown in Fig 1. Among them, the radial component p will cause tensile stress along the rebar surface in the concrete, leading to concrete cracking, while the longitudinal component τ is the bond strength that we would care about.

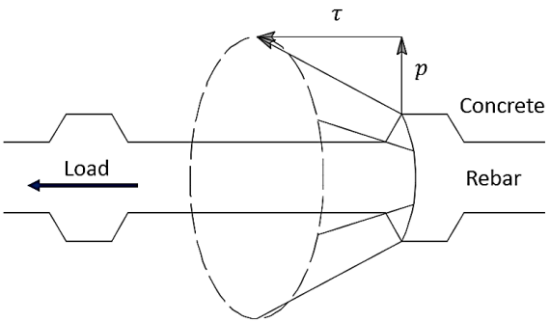

Fig 1. Bonding Force Mechanism

The difference in cracking modes is because the increase of confining pressure around rebar could weaken the splitting force σ_n, as shown in Fig 2. In the case of light constraints, splitting failure occurs, while heavy constraints will lead to the shear failure. The constraints effect will be affected by various factors, including the thickness of the protective layer of the concrete, the degree of corrosion and the loading method.

The bond force τ transfers the load to the concrete, at the same time, causes a large tensile stress concentration at the front ribs of the ribs, leading to internal diagonal cracking (Goto, 1971, Park, 1985). For shear failure, shear fracture occurs along the cylindrical slip surface of the steel rib outline, resulting in shear cracks (Park, 1975).

When the concrete crack fractures, the crack develops further along the weak surface between the aggregates, resulting in the rough and uneven fracture surface. The fracture surface will open and slip during the sliding process, and the exposed aggregates would extrude each other, resulting in tangential friction, transmitting shear force at the same time (Li, 1989).

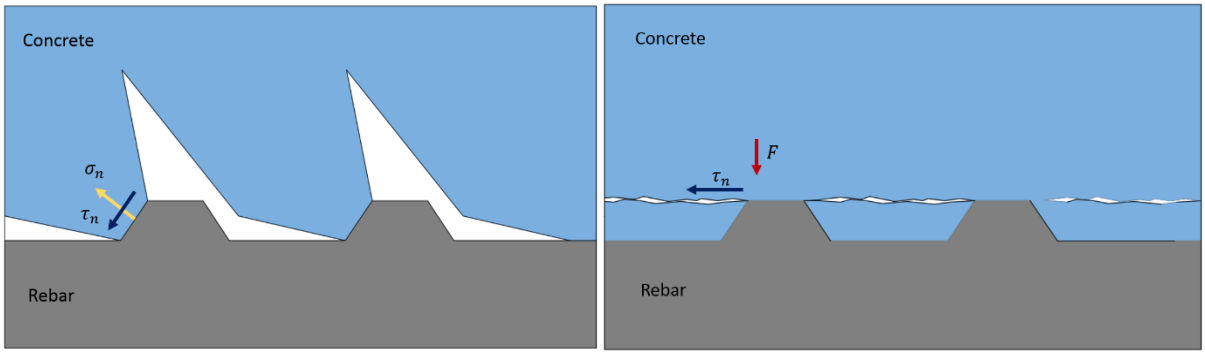

(a) (b)

Fig 2. (a) Splitting Failure Mechanism (b) Shear Failure Mechanism at Steel-concrete interface

In this study, based on the acoustic emission signal processing, the relationship between damage and acoustic emission under the influence of corrosion was established to provide a certain reference for the structural evaluation of corrosion damage.

METHODS

Experimental Methods

Specimens

A total of 24 concrete cubic samples of 150 mm were prepared, each with a 12mm steel rebar embedded in the centre as shown in Fig.3.

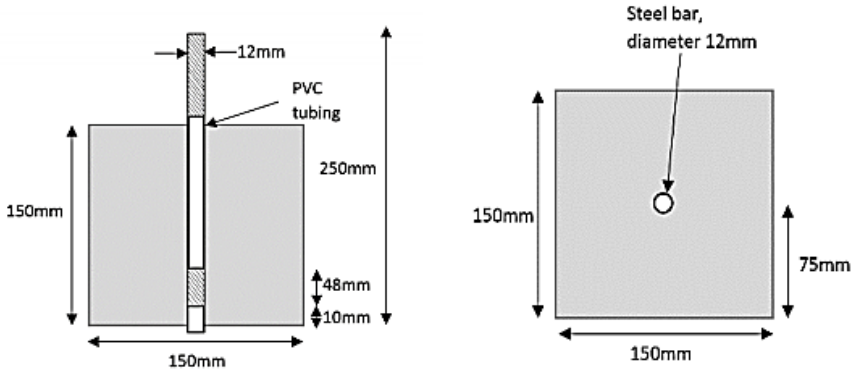

Fig 3. Specimen Design

The rebars were of standard type high deformed bars with 500 MPa of characteristic yield strength, complying with EN10080. To limit the area of corrosion exposure and bond strength, the rebars were covered by PVC tubes in concrete, leaving only a length of 48 mm being in direct contact with concrete. The upper and lower ends of the rebars were covered with the tubes as well, so that the corrosion would start from the inside of the concrete. The concrete mix design for this study adopts the BRE approach for design (Teychenné et al., 1975), as shown in Table 1.

Table 1. Concrete Mix Design

Water/Cement Ratio	**Slump(mm)**	**Fine Aggregates** (kg/m^3)	**Coarse Aggregates** (kg/m^3)	**28-Day Strength(MPa)**
0.47	45	529	940	30

Accelerated Corrosion

The specimens were air cured at room temperature for 28 days. After curing process, the specimens were placed inside a container with 5% sodium chloride solution. A DC power source for accelerated corrosion, as shown in Fig 4, was used. The DC power supply generated the voltage of 15.5V with 2A was used to connect the rebar of each specimen (anode) and a copper tube (cathode). The time of accelerated corrosion varied for each specimen to result in different levels of corrosion damage. It is noted that two specimens were allocated as the control specimens where no corrosion was induced.

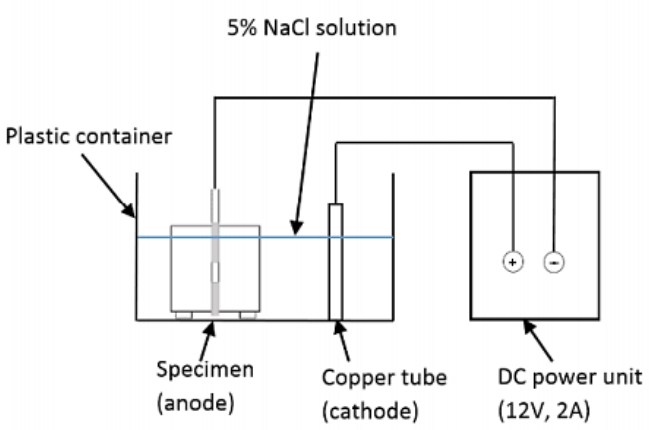

Fig 4. Accelerated Corrosion Set-up

Corrosion Level Measurement

It was then decided to use Archimedes principle to obtain the mass loss of the bonded lengths only (Chung, et al., 2008). The two ends of the bonded area were marked onto each sample bar, and then water was filled to the bottom mark. Mass readings began from zero at this point, as it was only the differences from the bonded length that were needed. The water was then filled to the higher end of the bond, and this mass was recorded for each bar. A control bar that had not been used within any specimens was used as the comparison mass (Chung, et al., 2008). The difference in mass between the specimen bars and the control bar was found, and this was taken as the mass loss of the bonded length. The original mass of the bonded section was measured using a 48mm piece of rebar.

Pull-out Test and AE Monitoring

It is also known that concrete structures will regularly be subjected to cyclic loading conditions throughout their service life (Sagar et al., 2015), and therefore by performing this type of test, data collected will better represent conditions that structures in actual service conditions. Loads will be applied manually through a computer system using a displacement-time method. A universal testing machine (Instron 4505) was used to test the capacity of specimens under static and cyclic pull-out.

A set of 10 specimens were statically loaded, while the remaining 10 specimens were subjected to cyclic loading. Displacement control loading with a loading rate of 0.2 mm/min was adopted in all tests. The first set, 10 specimens were pulled out monotonously to obtain the maximum bond strength and loading curve with different corrosion levels. After that, the remaining 10 specimens were loaded in cyclic with a load step programme shown in Fig 5 (ACI 437R-3).

In our experiment, the hole on the steel plate, which let the rebar go through, only occupies 8% of the contact surface area, it can be considered that the specimen was subjected to the full constraint of the upper and lower surfaces during the loading process.

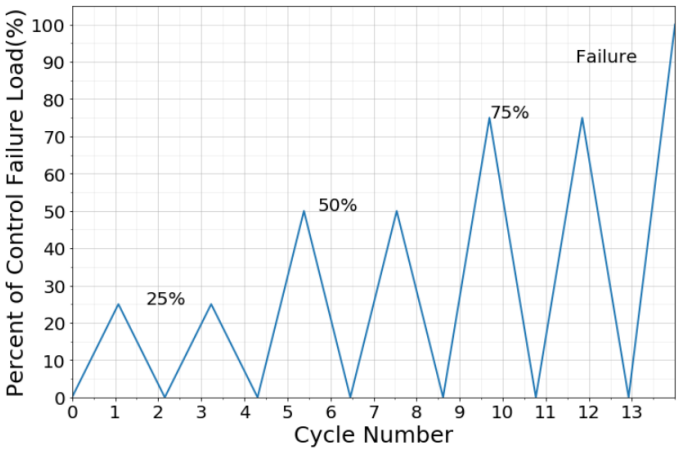

Fig 5. Steps for Cyclic Load Test

A four-channel AE measurement system (SAEU2S) was used to monitor fracture development during static and cyclic tests. It has the ability of real-time AE feature parameters extraction. The continuous acoustic emission feature parameter data receiving rate is greater than 400,000 groups/s, and it can implement hardware real-time FFT analysis as well. Four AE sensors of type SR150M with resonance 150 kHz and bandwidth 60 kHz ~ 400 kHz were used. AE measurement was configured with the parameters in Table 2. A digital displacement transducer, which was positioned by a grip fixed on the other end to the upper part of rebar, was placed in direct contact with specimen top surface for measure displacement during loading, as shown in Fig 6. The distance between the sensor and its nearest edges was 3 cm.

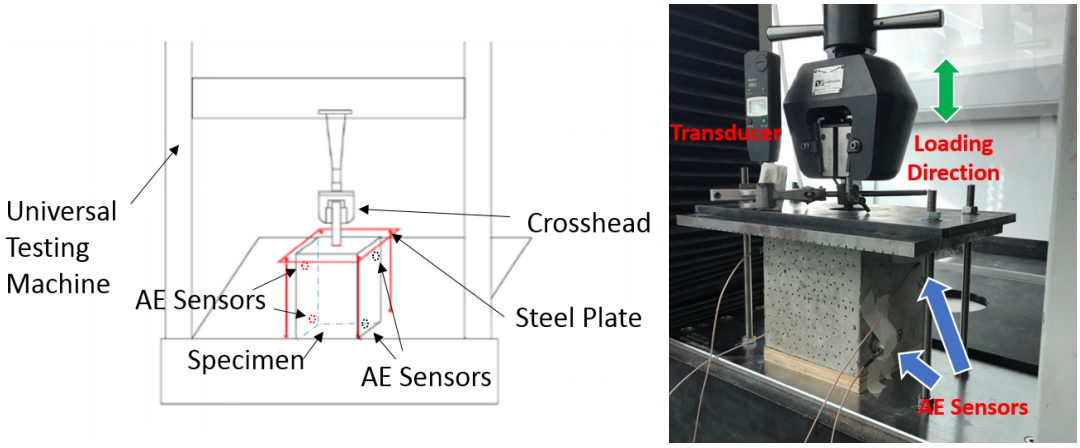

Fig 6. AE Layout for Accelerated Corrosion and Pull-out Testing

Table 2. AE Parameters

Wave Threshold (dB)	Pre-amplifier Gain (dB)	Frequency Filter (kHz)	Pre-amplifier (dB)
35	40	100 ~	40

Damage Evaluation

Damage Index

Based on continuum mechanics principles, damage parameter can be calculated as follows (Murakami, 2012),

$$\Omega_c = 1 - E/E^* \tag{1}$$

where E is the secant modulus, E^* is the tangent modulus and t is the signal time. Fig 7 illustrates the damage accumulation process corresponding to the change of the elasticity during test.

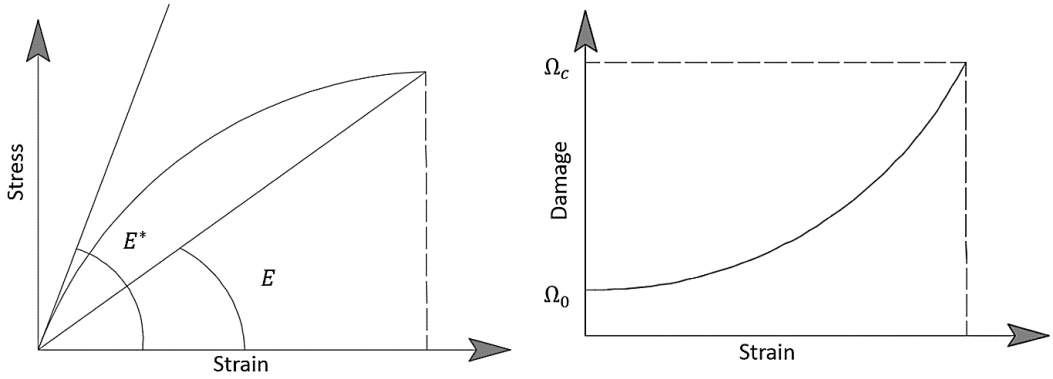

Fig 7. Stress Strain Relation and Damage Evolution Process

Damage Process Description

Previous findings suggest that there were two kinds of events happening during the pull-out test on the contact surface between rebar and concrete, namely the shear fracture and friction. It is considered that the former one generates primary AE signals, which dominates the damage process.

Using equations below can distinguish fracture events by enlarging the magnitude of the events which have high frequency and amplitude to describe shear fracture process. Two-step calculation was carried out. First, the frequency spectrum and frequency spectral centroid of each waveform signal were calculated by equation (2) and (3). Then equation (4) was used to increase AE signal sensitivity, which involves multiplication of frequency and amplitude to highlight high frequency and high amplitude events.

$$f(k) = \sum_{n=0}^{N-1} x_n e^{-\frac{i2\pi kn}{N}} \quad k = 1,2,3,\dots,N \tag{2}$$

$$FSC(k) = \frac{\sum_{k=0}^{N-1} f(k)x(k)}{\sum_{k=0}^{N-1} x(k)} \quad k = 1,2,3,\dots,N \tag{3}$$

This is followed by multiplying the FSC with Amplitude using equation (4), where N is total signal number.

$$AFSC(k) = Amplitude(k) * FSC(k) \quad k = 1,2,3,\dots,N \tag{4}$$

Total Damage Based on AE

To establish the relationship between traditional damage index Ω and AE-based damage description, the following equations are proposed in this study as given by equations (5) and (6). The cumulative damage signal analysis of specimens is to pick the maximum AFSC per minute, and calculate the integral the maximums over time.

$$MAFSC(n) = \max_{n<t<n+60} AFSC\,, n = 1,2,3 \ldots \left\lfloor \frac{T}{60} \right\rfloor \quad (5)$$

$$DA = \frac{\int_0^T MAFCS(n)\,dt}{T}, n = 1,2,3 \ldots \left\lfloor \frac{T}{60} \right\rfloor \quad (6)$$

Where t is signal time and T is the total time of sampling process.

RESULTS & DISCUSSION

Test Observation

From experimental findings, a total of 18 specimens showed shear failure mode, and only 2 specimens exhibited splitting failure mode, as exemplified in Fig 8. It was noticed that there was displacement difference between the transducer and testing machine. The difference was possibly due to the slight deformation of loading plate at the initial phase of loading. This caused the concrete specimen to be pulled up as one whole piece before equilibrium was reached, as observed during testing. The slip between rebar and concrete only occurred after a short while, then the fracture of steel-concrete interface started to generate AE signals.

Fig 8. Specimens after Pull-out

The frequency spectrum of AE signals obtained during testing is exemplified in Fig 9. It can be seen that the main frequency band is between 0-400kHz and the peak frequency of different signals varies from 150 kHz to 250 kHz.

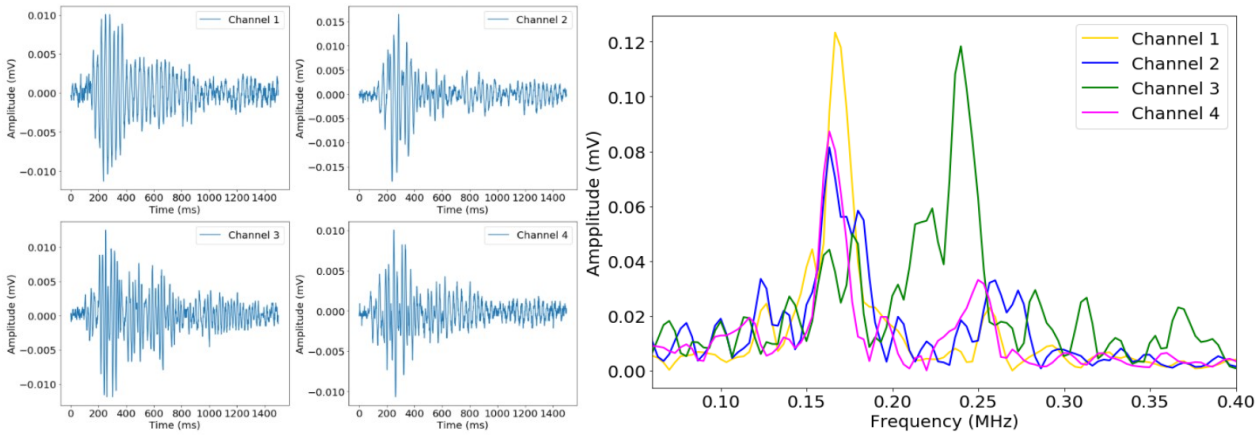

Fig 9. Raw AE Waveforms and Frequency Spectrum (2.40% Corrosion Level Specimen)

Bond Slip Behaviour and Corrosion Level

It can be seen that the loading curves all went through two phases, namely the linear growth phase and the descending phase. With respect to the shear failure, the curve in descending phase of splitting failure is very steep, nearly vertical, as can be seen in Fig 10.

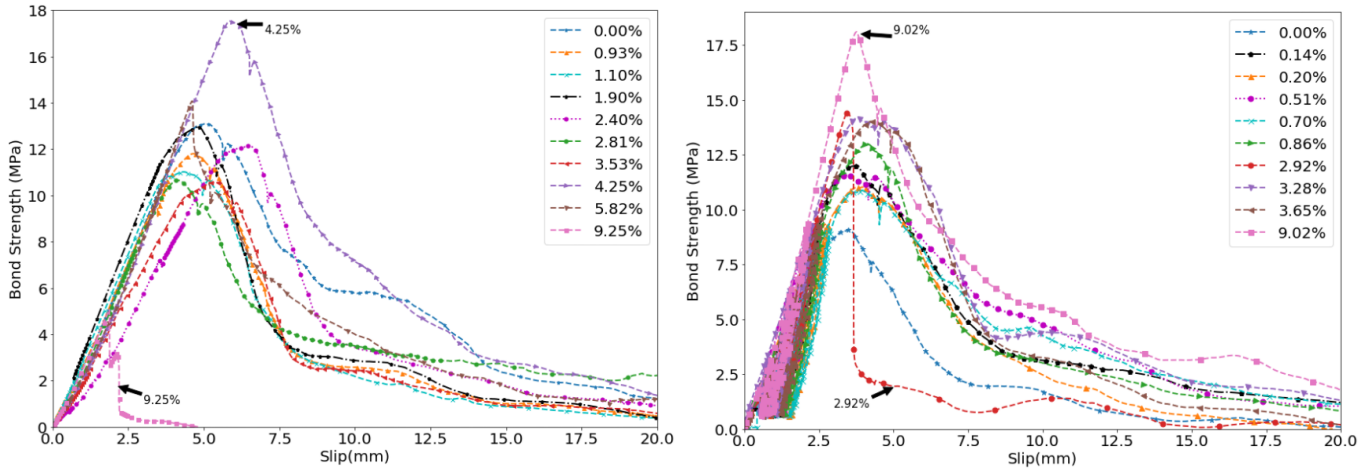

(a) Static Testing (b) Cyclic Testing

Fig 10. Slip vs Bond Strength in Static and Cyclic Testing

The data from pull-out testing suggested that, when the corrosion level is about 4%-7%, the bond strength was increased due to the rust expansion. The increase of bond strength at a relatively low level (4%-7%) is due to the rise of radial stress and friction. When the corrosion was further developed, for example, exceeds 7%, the bearing capacity may have a trend of significantly decrease, Fig 11(a). The stress increasing caused by the accumulation of corrosion products could eventually reduce the bearing capacity.

The work of external force was calculated using the integral of force over displacement. Regression line from Fig 11(b) exhibit the same trend of work versus corrosion level, both having the rising phase and the dropping phase, reaching the maximum at a corrosion level around 4% corrosion level.

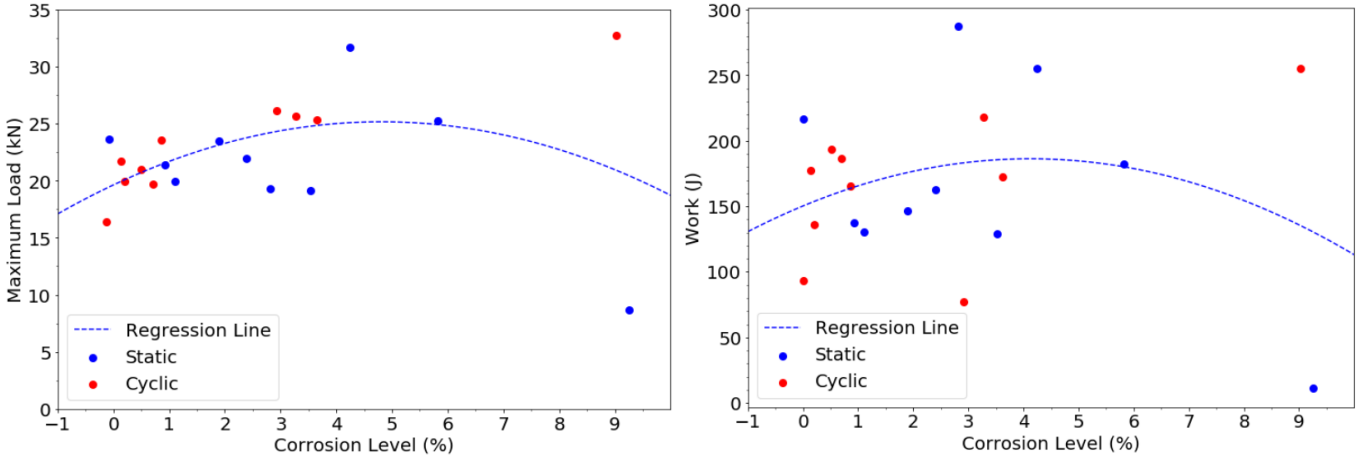

(a) Maximum Load (b) Work

Fig 11. Corrosion Level vs Maximum Load and Work

Damage Description by AE

As can be seen from Figure 12(a), the friction signal was depressed while the shear fracture signal was amplified. The new parameter, AFCS, could reflect the process of shear damage during the pull-out test. Based on this, it can be seen that AE signal did not appear at the beginning of loading while after the slight

deformation phase, signals began to generate. A large number of concrete shear fractures occurred in the rapid descending phase.

When the AFCS reaches a relatively high value (> 25 dB MHz), it indicates that the concrete had a shear crack, while the relatively low values (<25 dB MHz) implies the friction events in the test. At the same time, the growth trend of AFCS (dotted line in black) is similar to the traditional damage expression (the green line).

It can also be seen from the Fig 12(b), the AE total damage description, DA, is having a good positive correlation with the external force work. It could be used for damage statistics from the view of AE method.

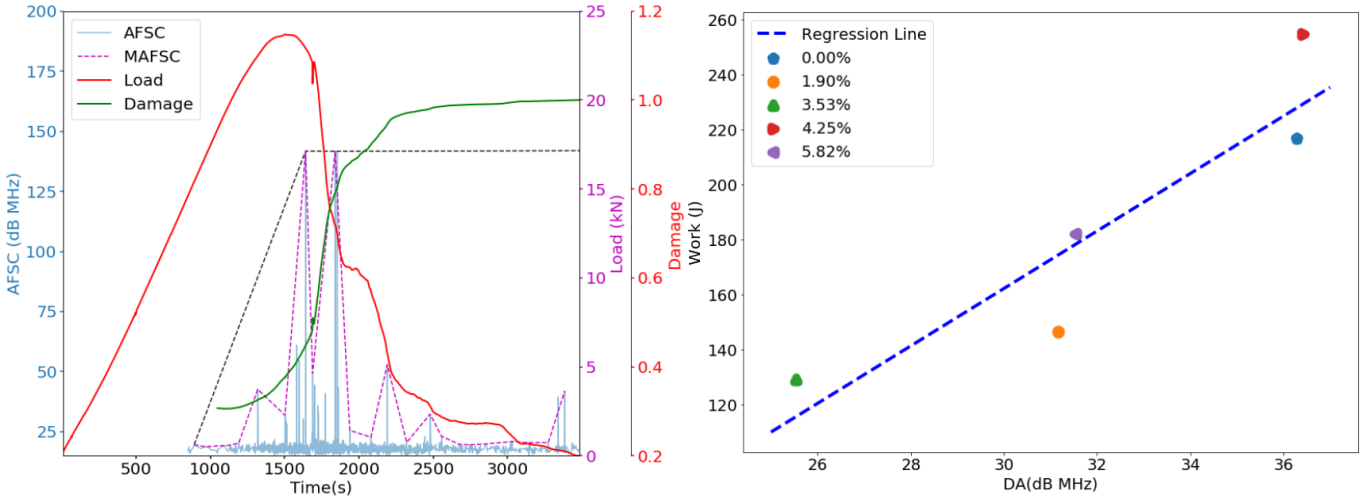

(a)Damage Process (b)Work vs DA

Fig 12. Damage Process and Relation between Work and DA

CONCLUSION

By a series of experiments and data analysis, several conclusions about the corrosion effect on the bond strength and the characteristics of the acoustic emission signal in the experimental process were revealed.

Corrosion Effect on Bond Strength

The experiment can explain the effect of corrosion on the bond strength that a relatively low corrosion level (4%-7%) could enhance bond strength in monotonous loading due to the expansion of corrosion products, and when corrosion level continued to grow, it could gradually weaken bond strength.

Damage Description Based on AE

Through the analysis and presentation of the AE data, the new AE parameters MAFCS and DA were showing a good correlation with the traditional damage parameters (W and Ω) during the pull-out testing. The MAFCS could be used to distinguish and highlight the concrete shear fracture, thus, providing a reference for the RC structures damage description.

FUTURE WORK

A thorough analysis of AE data from the cyclically loaded specimens is required to examine the sensitivity of the DA to the loading method.

REFERENCE

Stewart, M. G., & Rosowsky, D. V. (1998). Structural safety and serviceability of concrete bridges subject to corrosion. Journal of Infrastructure systems, 4(4), 146-155.

Nawy, E. (2000). Reinforced concrete: A fundamental approach.

Golaski, L., Gebski, P., & Ono, K. (2002). Diagnostics of reinforced concrete bridges by acoustic emission. Journal of acoustic emission, 20(2002), 83-89.

EN10080, U. N. I. "Steel for the reinforcement of concrete–weldable reinforcing steel 25." (2005).

Teychenné, D. C., Franklin, R. E., Erntroy, H. C., & Marsh, B. K. (1975). Design of normal concrete mixes. HM Stationery Office.

Chung, L., Kim, J. H. J., & Yi, S. T. (2008). Bond strength prediction for reinforced concrete members with highly corroded reinforcing bars. Cement and concrete composites, 30(7), 603-611.

Sagar, R. V., & Rao, M. V. M. S. (2015). Acoustic emission during flexural deformation of reinforced concrete under incremental cyclic loading. Journal of Testing and Evaluation, 44(6), 2182-2198.

Park, Y. J., & Ang, A. H. S. (1985). Mechanistic seismic damage model for reinforced concrete. Journal of structural engineering, 111(4), 722-739.

Park, R., & Paulay, T. (1975). Reinforced concrete structures. John Wiley & Sons.

Goto, Y. (1971, April). Cracks formed in concrete around deformed tension bars. In Journal Proceedings (Vol. 68, No. 4, pp. 244-251).

Li, B. (1989). Contact density model for stress transfer across cracks in concrete. Journal of the Faculty of Engineering, the University of Tokyo, (1), 9-52.

Ohtsu, M. (1987). Acoustic emission characteristics in concrete and diagnostic applications. Journal of Acoustic Emission, 6(2), 99-108.

Grosse, C., Weiler, B., & Reinhardt, H. W. (1997). Relative moment tensor inversion applied to concrete fracture tests. J. of Acoustic Emission, 14(3-4), S64-S87.

Yalciner, H., Eren, O., & Sensoy, S. (2012). An experimental study on the bond strength between reinforcement bars and concrete as a function of concrete cover, strength and corrosion level. Cement and Concrete Research, 42(5), 643-655.

Saether, I. (2011). Bond deterioration of corroded steel bars in concrete. Structure and Infrastructure Engineering, 7(6), 415-429.

Murakami, S. (2012). Continuum damage mechanics: a continuum mechanics approach to the analysis of damage and fracture (Vol. 185). Springer Science & Business Media.

Wang, X., Ge, H., Song, L., He, T., & Xin, W. (2011). Experimental study of two types of rock sample acoustic emission events and Kaiser effect point recognition approach. Chinese Journal of Rock Mechanics and Engineering, 30(03), 580-588.

American Concrete Institute (ACI), 2003. 437R - 03: Strength Evaluation of Existing Concrete Buildings. pp. 1-28.

American Society of Civil Engineers (ASCE), 2017. Bridges.

BS 1881-113:2011: Testing concrete. Method for making and curing no-fines test cubes, 2011

Supplementary Data

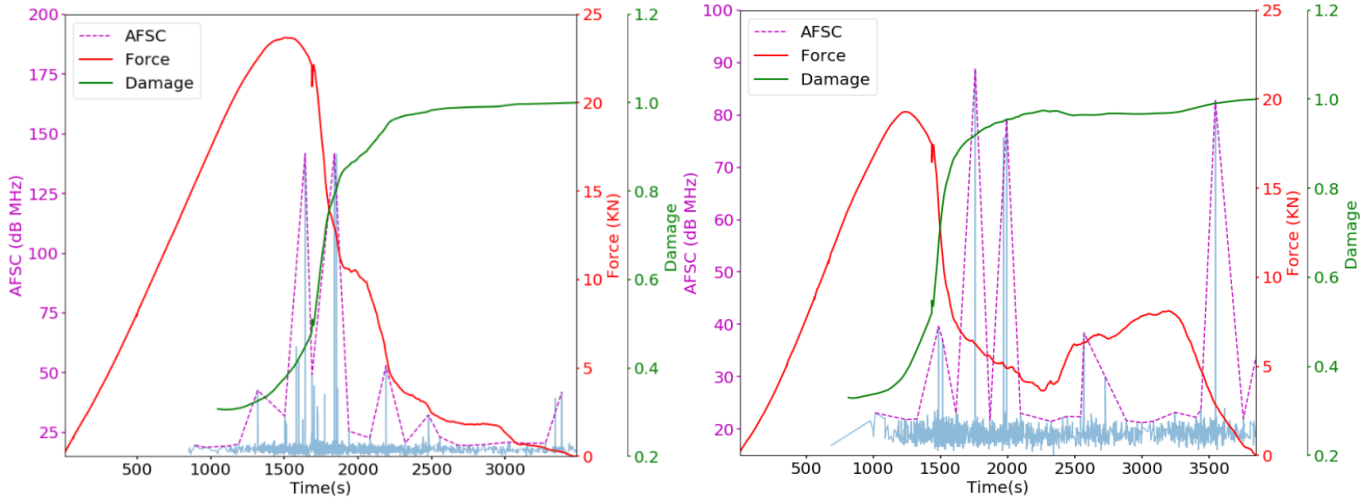

(1)

(2)

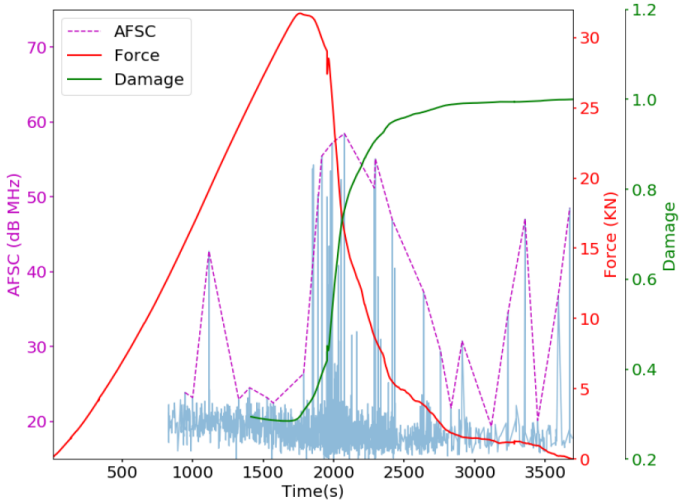

(3)

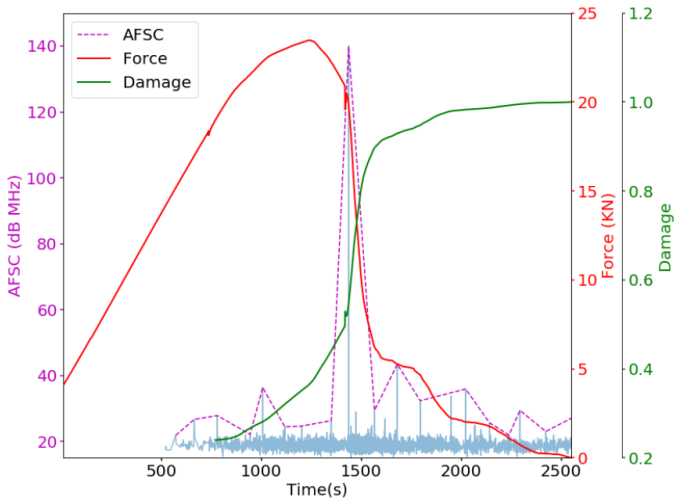

(4)

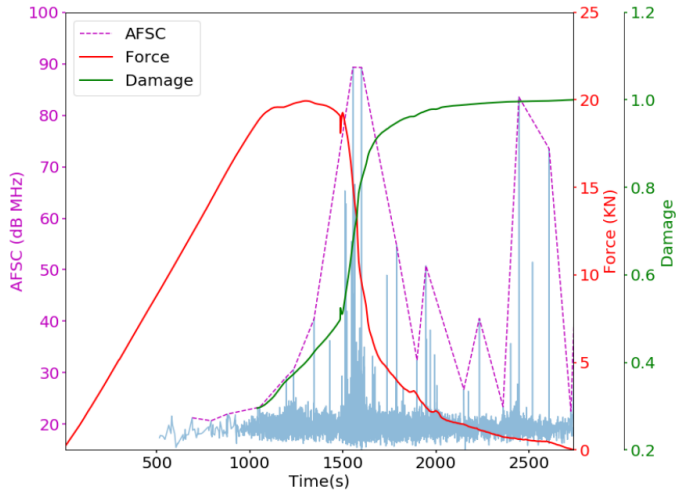

(5)

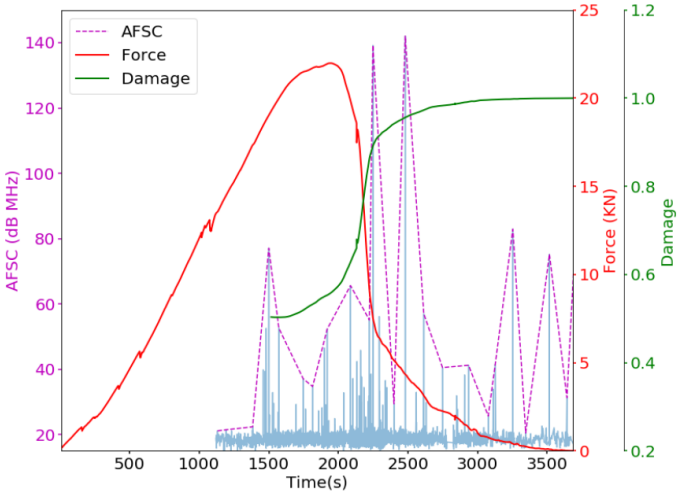

(6)

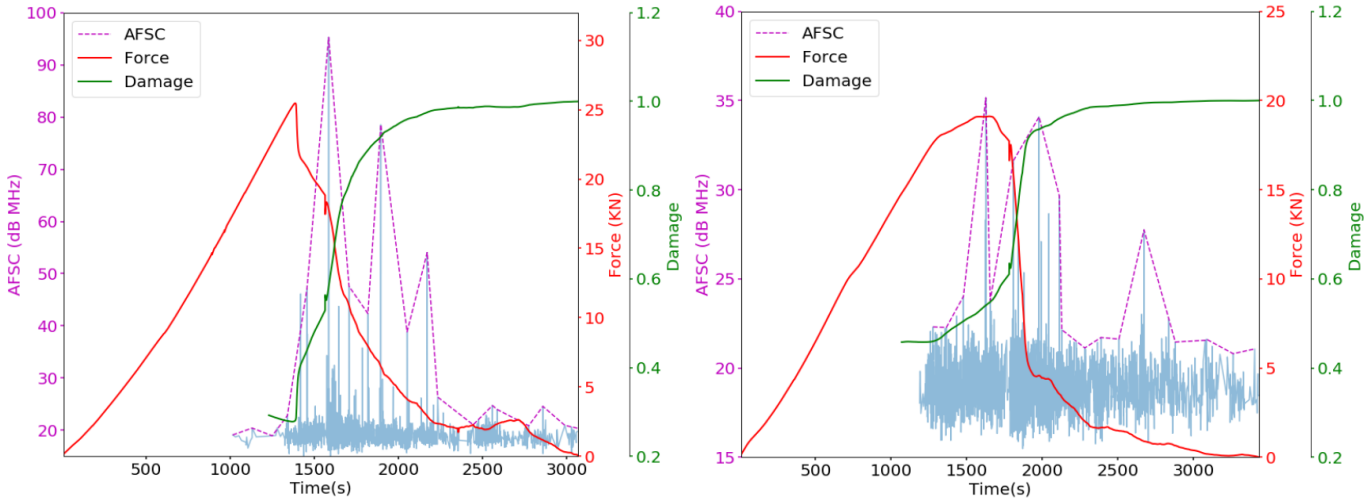

(7) (8)

Fig 13. AE Signals of Different Specimens